mater.scichina.com link.springer.com

Published online 8 September 2021 | https://doi.org/10.1007/s40843-021-1765-x
Sci China Mater 2022, 65(3): 780–787

Coexistence of large positive and negative magnetoresistance in $Cr_2Si_2Te_6$ ferromagnetic semiconductor

Zhou Li[1†], Wei Bai[1†], Yuliang Li[3], Yuanlong Li[1], Sheng Wang[3], Weihui Zhang[1], Jiyin Zhao[1], Zhe Sun[3], Chong Xiao[1,2*] and Yi Xie[1,2]

ABSTRACT **Magnetoresistance (MR) phenomenon couples the electron transport with magnetic field, which has been at the forefront of condensed matter physics and materials science. Large-MR behaviors are of particularly importance for magnetic sensor and information memory applications, and their scarcity has aroused intensive research. Moreover, due to the different physical origins, combination of large positive and negative MR (pMR and nMR) in one single compound has rarely been reported. In present work, we achieved a coexistence of large pMR and nMR in $Cr_2Si_2Te_6$ ferromagnetic semiconductor single crystal with different field configurations. Specifically, a large nMR of about −60% was obtained under the in-plane field, while a large pMR higher than 1000% took over in the out-of-plane direction. We attribute this field direction-sensitive dualistic large MR behavior to the competition and cooperation effect from the ferromagnetic interaction, orbital scattering and electronic correlation that coexist in $Cr_2Si_2Te_6$, which contribute to nMR, pMR, and nMR, respectively, in dominated temperature and field ranges, and show different weights under different field directions. The elucidated multiple MR mechanism in this ferromagnetic semiconductor will shed light on the pursuit of coexistence of large pMR and nMR for field-sensitive device applications.**

Keywords: large pMR and nMR, dualistic magnetoresistance, $Cr_2Si_2Te_6$, ferromagnetic semiconductor, single crystal

INTRODUCTION

Magnetoresistance (MR) describes the tendency of a material to change the value of its electrical resistance in an externally applied magnetic field, which couples the electron transport with magnetic field [1], and has always been at the cutting edge of condensed matter physics, solid-state chemistry and materials science [2,3]. In terms of application, materials that exhibit large MR (whether positive or negative), like giant MR (GMR) and colossal MR (CMR) [4–7], have already found use in devices such as magnetic sensors and memories [8,9], as well as hard drives [10]. However, large-MR phenomena and materials are uncommon, which motivates us to explore new and potential candidates for further progress in this field. Moreover, considering the field-sensitive device applications, hunting for material systems that combine large positive and negative MR (pMR and nMR) together is of great significance. However, due to the different origins of large pMR and nMR, coexistence of them in a single compound has rarely been reported. Large pMR mainly comes from the compensation effect or ultrahigh carrier mobility in nonmagnetic semimetals [11,12], while large nMR is usually found in artificially ferromagnetic (FM) multilayer systems with magnetic coupling interaction [4,5], or manganite perovskites arising from the interaction between the conduction and localized electron spins in different orbitals [6,13,14]. Thus, the different physical and chemical origins, and the corresponding material systems make it quite challenging to acquire both large pMR and nMR.

Intrinsically FM semiconductors (FMS's) with both ferromagnetism and semiconductor features hold great promise for fundamental physics and future applications in spintronics [15,16]. Among them, van der Waals (vdW) FMS's, like $Cr_2X_2Te_6$ (X = Si, Ge) and XI_3 (X = Cr, V) have received intense concern due to their 2D vdW lattice coupled with ferromagnetism [17–23], which is beneficial to studying the origin and implication of magnetic interaction in few/mono-layer crystals, as well as novel spintronic vdW heterostructures [24]. More importantly, due to the crystal anisotropy, layered FMS's can exhibit magneto-crystalline anisotropy, which may offer an opportunity for achieving both large pMR and nMR. Therefore, it is rewarding to explore the MR behavior in vdW FMS for the sustainability of this burgeoning field. As a typical vdW FMS, bulk $Cr_2Si_2Te_6$ shows 2D Ising-like FM behavior with the Curie temperature (T_c) of 32–34 K [25,26]. It has a layered structure which contains [Te–$Cr_{2/3}(Si_2)_{1/3}$–Te] sandwich layers stacking along c axis (see Fig. 1a). The infrequent [Si_2Te_6] ethane-like groups locate at the center of the hexagons formed by [$CrTe_6$] octahedron, which is reported to be responsible for $Cr_2Si_2Te_6$'s molecular-like sharp and localized electronic density of states (DOS) [27]. In the meantime, $Cr_2Si_2Te_6$ also exhibits magneto-crystalline anisotropy due to its crystal anisotropy, which spurs us to learn more about its anisotropic magnetotransport properties.

Here, we uncover the magnetotransport behavior of $Cr_2Si_2Te_6$ single crystal with strong MR anisotropy between the in-plane

[1] Hefei National Laboratory for Physical Sciences at the Microscale, CAS Center for Excellence in Nanoscience, University of Science and Technology of China, Hefei 230026, China
[2] Institute of Energy, Hefei Comprehensive National Science Center, Hefei 230031, China
[3] National Synchrotron Radiation Laboratory, University of Science and Technology of China, Hefei 230029, China
† These authors contributed equally to this work.
* Corresponding author (email: cxiao@ustc.edu.cn)

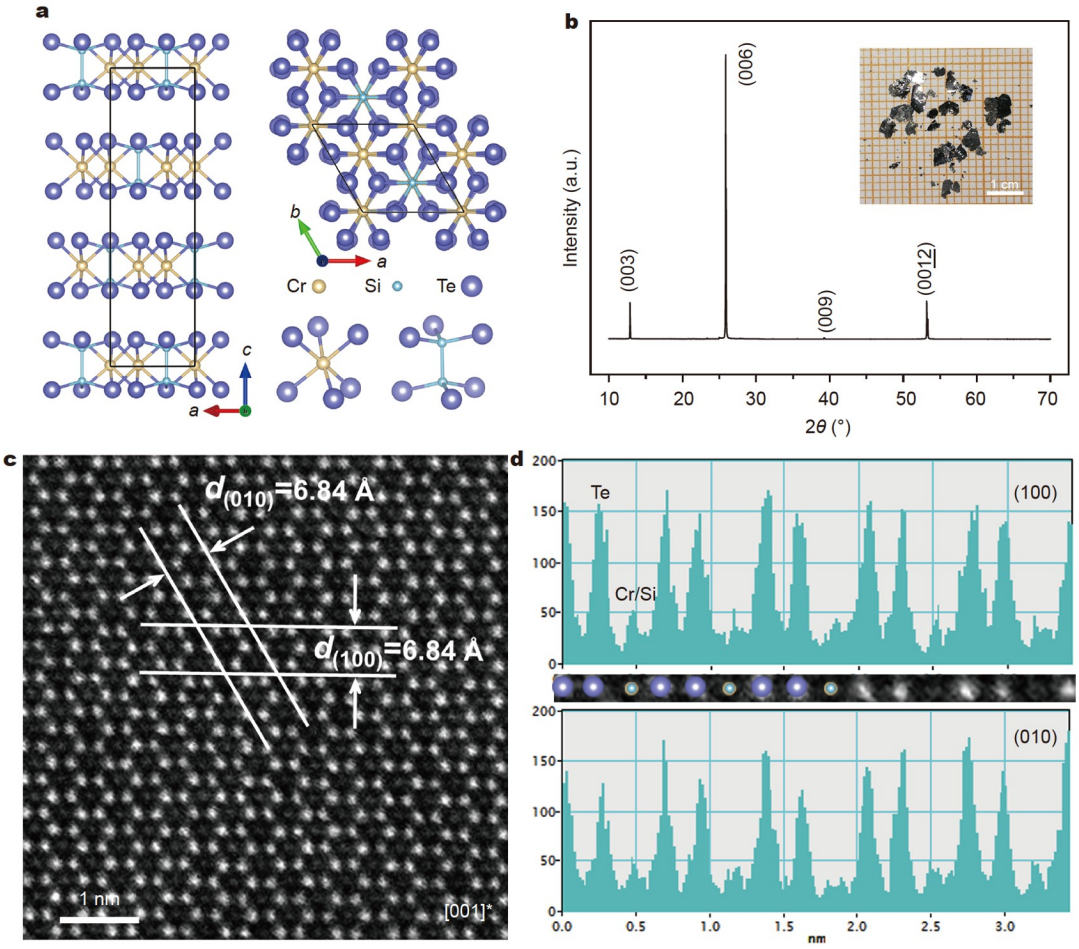

Figure 1 Structure and phase characterizations. (a) Schematic crystal structure of $Cr_2Si_2Te_6$ along the [010] and [001] directions, with the [$CrTe_6$] octahedron and ethane-like [Si_2Te_6] species. (b) XRD patterns for a piece of $Cr_2Si_2Te_6$ single crystal. Inset: the optical photograph. (c) HAADF-STEM image of $Cr_2Si_2Te_6$ single crystal obtained along the [001] direction. (d) Intensity profiles along the [100] and [010] axes, respectively.

($H\|ab$) and out-of-plane ($H\perp ab$) magnetic field directions, and acquire the coexistence of large pMR and nMR under different field configurations. Specifically, a large nMR of about −60% is obtained below 22.5 K under ~1 T and $H\|$ field. Nevertheless, as soon as the field is rotated to $H\perp$ direction, this large nMR is overwhelmed by the emergence of a pronounced pMR, and a large pMR higher than 1000% takes over at temperatures around T_c. A competition and cooperation mechanism among FM, orbital and electronic correlation is proposed to explain the unusual and intriguing MR behavior observed in $Cr_2Si_2Te_6$. FM, orbital and electronic correlation contribute nMR, pMR, and nMR, respectively, in dominated temperature and field ranges, and show different weighted contribution of positive and negative sources under different field directions. This multiple MR mechanism elucidated in present work will deepen our understanding of the microscopic magneto-transport process and shed light on the pursuit of qualified materials for field-sensitive device applications.

EXPERIMENTAL SECTION

Materials and synthesis

Cr powder (3N), Si powder (3N), and I_2 (4N) were purchased from Sinopharm Chemical Reagent Co., Ltd.; Te powder (4N) was purchased from Shanghai Aladdin Biochemical Technology Co., Ltd. All chemicals were used as received without further purification.

$Cr_2Si_2Te_6$ single crystals were grown by a chemical vapor transport (CVT) method. A stoichiometric mixture of Cr, Si, Te powders was sealed in evacuated silica tubes with I_2 as the transport agent according to the amount of 5 mg cm^{-3}. The starting materials were then placed inside a two-zone furnace to react over a period of 7 days between 923 and 1123 K, and then naturally cooled to room temperature. After the reaction, a fine dark-grey crystalline powder was obtained, within which some small lamellar crystals with silver metallic luster could be found.

Characterizations

The X-ray diffraction (XRD) data were taken with Cu Kα (λ = 0.15418 nm) radiation using a Rigaku Dmax diffraction system. The microstructure and element analysis were performed on a JEOL JSM-6700F scanning electron microscopy (SEM) system with energy-dispersive X-ray spectroscopy (EDS), confirming a stoichiometric $Cr_2Si_2Te_6$ single crystal. High-resolution transmission electron microscopy (HRTEM) images and high-angle annular dark-field scanning TEM (HAADF−STEM) images were

collected on a spherical aberration-corrected JEOL ARM-200F field-emission transmission electron microscope.

Physical property measurements

The magnetic measurements were performed on a Quantum Design MPMS-XL3 system in a temperature range from 4 to 200 K with a temperature step of 2 K and magnetic fields up to 5 T. The magnetotransport properties were performed on a Quantum Design PPMS system (PPMS®DynaCool™) using Horizontal Rotator Option in the temperature range of 20–300 K with the magnetic field up to 14 T. "Direct current (DC) resistivity" mode was used in the high-temperature range (above 50 K) while "electrical transport option (ETO)" mode was used in the low-temperature range (below 50 K), because the resistance increases sharply at low temperatures and exceeds the test range when using four-point "DC resistivity" mode. Electrical contacts were prepared by indium welding with a two or four-probe configuration depending on the electrical transport measurement modes. Single crystals with typical dimension of $2.5 \times 1.5 \times 0.3\ mm^3$ were used in magnetotransport properties. Repeated experiments on different crystals showed similar behavior, confirming the results presented in this paper.

ARPES measurements

Angle resolved photoemission spectroscopy (ARPES) experiments were performed with 20-eV photons at the beam line 13U of the National Synchrotron Radiation Laboratory (NSRL) in Hefei, China, using a Scienta R4000 electron spectrometer. The angular resolution was 0.3°, and the combined instrumental energy resolution was higher than 20 meV. All samples were cleaved *in situ* and measured under a vacuum higher than 8×10^{-11} mbar.

RESULTS AND DISCUSSION

Structure and composition characterizations

Single crystals of $Cr_2Si_2Te_6$ were obtained by the CVT method, which are small mirror-like shinning platelets with lateral dimensions of several millimeters (inset in Fig. 1b). The clear and sharp (00*l*) peaks observed from XRD patterns (Fig. 1b) indicate that the surface of the crystal is normal to the *c* axis. EDS analysis of the platelet gives an element composition of 2:2.01:6.04 (see Table S1), very close to the stoichiometry of $Cr_2Si_2Te_6$. Element mappings of $Cr_2Si_2Te_6$ single crystal (see Fig. S1) show homogeneous distribution of Cr, Si, and Te elements. The crystal structure viewed along [001] is illustrated by HAADF-STEM image in Fig. 1c. According to the *Z* contrast principle, the brighter points in Fig. 1c correspond to Te atom columns, which build up a hexagonal close packing, while the "-Cr-Cr-Si_2-" atom columns are inserted perpendicularly at each center position of the hexagons. Intensity profiles along the [100] and [010] directions (Fig. 1d) clearly feature alternate intense and weak peaks due to local variation of elements along the lines, as labeled in Fig. 1d. Lattice parameter with $a = b = 6.84$ Å can be easily obtained from the relative distance between the corresponding atoms, consistent with the theoretical values [25]. These results suggest that we have obtained high-quality $Cr_2Si_2Te_6$ single crystals.

Electrical and magnetic property characterizations

Fig. 2a presents the band structure of $Cr_2Si_2Te_6$ single crystals measured by ARPES at different temperatures. The identical dispersive features at 30, 50 and 100 K indicate that the valence band structure of $Cr_2Si_2Te_6$ remains unchanged with temperature variation and keeps consistency from the FM to paramagnetic (PM) phase, although there is a slight rigid shift to deeper binding energy in the spectrum taken at 30 K due to the charging effect. From the broad range dispersion along the *Γ*–*K* direction, we could identify both dispersive feature near the valence band maximum (VBM) and rather flat bands at ~1.5 eV below the VBM, consistent with the previous report [28]. This flat band leads to a sharp and localized electronic DOS, as indicated by the energy distribution curve (EDC) intensity derived from 30 K ARPES data (Fig. 2b), which is attributed to the $[Si_2Te_6]^{6-}$-like anion species as stated before [27]. The resistance of $Cr_2Si_2Te_6$ single crystal (sample 1, marked as #S1) was first investigated using four-probe "DC resistivity option" (Fig. 2c, black hollow data points), which increases monotonically as the temperature decreases and quickly exceeds the measuring range of instrument below 50 K. The data between 150 and 300 K can be fitted by the Arrhenius's equation, suggesting a thermal excitation electrical transport mechanism and the thermal activation energy E_{a1} is about 140 meV. Then, a high-impedance two-probe configuration (Fig. S2a) was further employed on the same single crystal with "ETO" (Fig. 2c, red solid data points). The resistance value obtained by ETO is in good agreement with the former below 70 K, and finally exceeds the measuring range again below ~20 K. Therefore, in present work, electronic transport data obtained by four-probe were adopted at temperatures above 50 K, while at temperatures between 20 and 50 K, data measured by two-probe were adopted. Hall coefficient measurement (Fig. S2b) was taken to determine the carrier concentration (n) and mobility (μ). However, due to quite obvious background of MR in the low-temperature range (as discussed below), only n data above 100 K are obtained and shown in Fig. 2d, which also follows the Arrhenius's law with a thermal activation energy E_{a2} of 141 meV, well consistent with the value of E_{a1}. The deduced μ is shown in Fig. S3, which follows a $T^{-3/2}$ dependence in the high-temperature range, suggesting the acoustic phonon scattering [29,30].

The magnetic property characterization results of $Cr_2Si_2Te_6$ single crystal are displayed in Figs S4 and S5. Fig. S4a, b show the temperature-dependent zero-field cooling and field-cooling magnetization (M–T) curves of the $Cr_2Si_2Te_6$ single crystal with $H\|$ and $H\perp$ field of 0.05 T. The T_c defined by the minima of the dM/dT curves (insets in the figures) is ~34 K. Due to the Cr–Te–Cr superexchange interaction at low temperatures [31], there is an apparent bifurcation in the M signal below T_c. Meanwhile, the large discrepancy on M value between $H\|$ and $H\perp$ directions signifies its large magnetic anisotropy and the easy *c*-axis [25,26,32]. In M–T curves of both $H\|$ and $H\perp$ field directions (see Fig. S4c, d), M increases with H, and is nearly isotropic at high fields while significantly anisotropic at low fields, which corresponds to the saturation behavior of magnetic moment at higher fields. In the FM state, the maximum value of magnetic moment reaches 2.925 and 2.997 μ_B per Cr atom at 4 K (see Fig. S5a, b), which is in excellent agreement with the 3.0 μ_B value expected for Cr^{3+} cations. The saturation field H_s ~0.20 T with $H\perp$ field is much smaller than the H_s ~1.25 T with $H\|$ field (see Fig. S5c, d). These results confirm the easy *c*-axis and large magnetic anisotropy in vdW FM $Cr_2Si_2Te_6$.

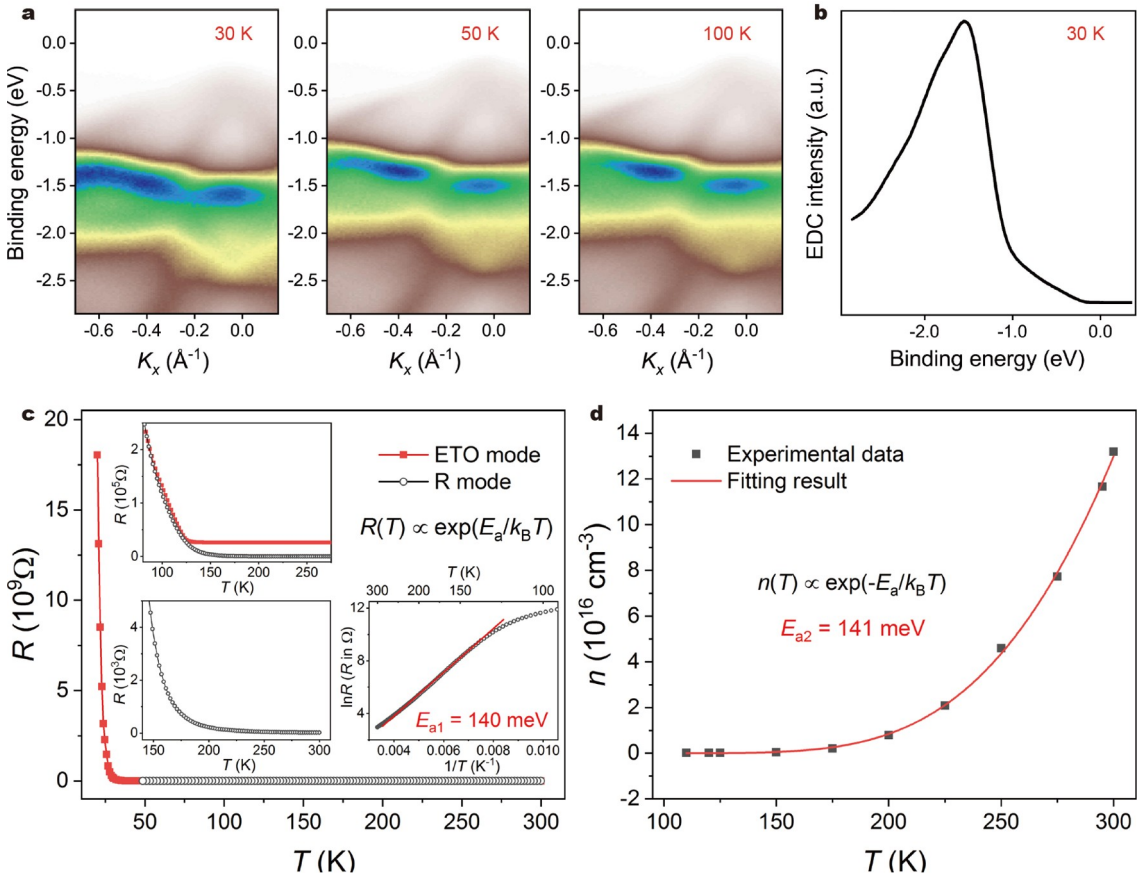

Figure 2 Electronic band structure and transport property characterizations. (a) Temperature-dependent band structures measured by ARPES along the *Γ*–*K* direction. (b) EDC intensity derived from the 30-K ARPES data. (c) Temperature-dependent resistance of $Cr_2Si_2Te_6$ measured by both two- and four-probe (ETO and DC resistivity) modes. Insets: enlarged displaying of the data and Arrhenius fitting of the DC resistivity-mode in the higher-temperature range. (d) The temperature-dependent *n* with fitting using Arrhenius's law.

Dualistic magnetotransport behavior and coexistence of large pMR and nMR

Due to the magnetic anisotropy, we explored the anisotropic magnetotransport behavior of $Cr_2Si_2Te_6$ under different field configurations. The *H*||*ab* direction field-dependent MR data are shown in Fig. 3a–c and Fig. S6. Under *H*||*ab* field configuration, the field-dependent MR shows a roughly "W" shape and experiences a change of sign from negative below T_c to positive above T_c at high fields while always keeping a notable nMR at low fields. Below T_c, a very large nMR dominates in a wide field range, and shows extremum (the lowest point of "W" line) at 0.75–1.50 T (see Fig. S6a, b). Typically, at 22.5 K, a large nMR of about −60% is obtained at ~1.0 T (Fig. 3b, extracted from the orange-red line in Fig. 3a), which becomes smaller and upwarps in the high-field range when the temperature rises to T_c, but still persists very small negative values in the low-field range (Fig. S6c). The *H* values corresponding to the extremum remind us the saturation field H_s with *H*||*ab* field (Figs S4c and S5c), which is exactly in the same field range, indicating that this low-field nMR is related to FM interaction. As for the high-field range below T_c, the magnetotransport is dominated by ordinary orbit scattering which shows a pMR and causes the upwarp of the curve. Above T_c, with the increase of temperature, the absolute values of both pMR and nMR become smaller (Fig. 3c and Fig. S6d). Meanwhile, the nMR-to-pMR transition points extends to higher fields, which results from the contribution of electronic correlation rather than FM interaction because the system goes into the PM state and only the electron interactions matter [28]. Finally, the signal disappears (covered by fluctuations) above 100 K. These results demonstrate that the FM interaction, orbital scattering and electronic correlation coexist in $Cr_2Si_2Te_6$, and contribute nMR, pMR, and nMR, respectively, in dominated temperature and magnetic field ranges. Among them, the more prominent FM interaction dominates below T_c in the low-field range and leads to the acquisition of larger nMR under *H*||*ab* field configuration.

When the magnetic field changes from *H*||*ab* to *H*⊥*ab* configuration, field dependences of MR are shown in Fig. 3d–f and Fig. S7. At temperatures below 50 K, a pMR is demonstrated in the whole test temperature and field ranges. Its value rises first and then falls with increasing temperature, and reaches a maximum around T_c (see Fig. 3d and Fig. S7c, d). Typically, at 32.5 K, a large pMR higher than 1000% is obtained at 14 T and shows no sign of saturation (Fig. 3e, extracted from the tan line in Fig. 3d). Compared with that of *H*||*ab* direction, the MR behavior in the *H*⊥*ab* direction seems to be quite different. However, when we look at the variation trend rather than absolute MR value, the MR mechanism behaves actually in the same way as in the *H*||*ab* direction. Specifically, below T_c, as shown in Fig. S7a, b, a "zero" MR phenomenon shows below the field of 0.2 T, which is exactly consistent with the saturation field H_s in the *H*⊥*ab* magnetization direction (see Figs S4d and S5d).

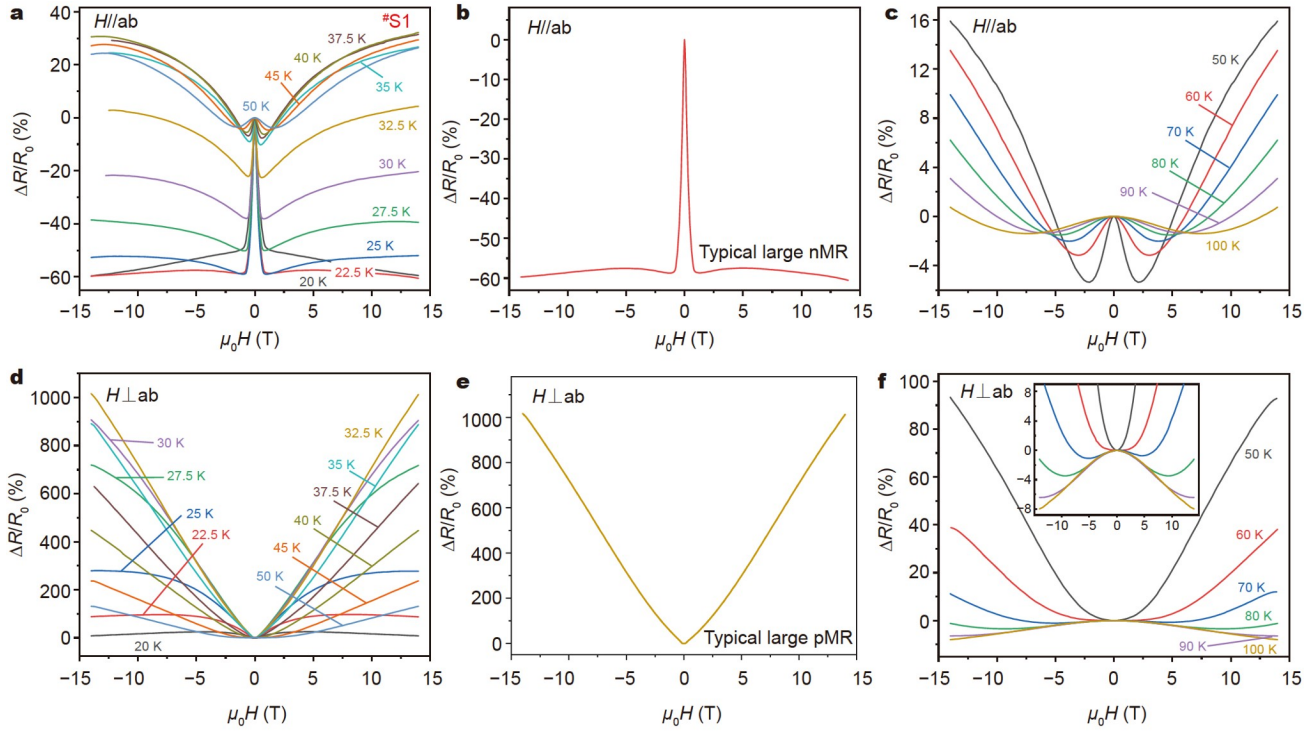

Figure 3 Magnetotransport behavior of $Cr_2Si_2Te_6$ single crystal. (a) The $H\|ab$ direction MR measured below 50 K using ETO. (b) Typical large nMR obtained at 22.5 K. (c) The $H\|ab$ direction MR measured above 50 K using DC resistivity option. (d) The $H\perp ab$ direction MR measured below 50 K. (e) Typical large pMR obtained at 32.5 K. (f) The $H\perp ab$ direction MR measured above 50 K. Inset: enlarged displaying to highlight the nMR at higher temperatures.

This indicates that the FM-contributed nMR also exists at low fields (like that in the $H\|ab$ direction); however, it is almost completely covered by the pMR of orbit scattering [33]. The anisotropic orbit scattering is the dominant contribution of the large pMR which may come from the electron scattering by the orbit of the first valence band (as shown in Fig. 4e), and causes much larger magnitude of pMR in the $H\perp ab$ field than in the $H\|ab$ field. When the temperature rises above 50 K, the pMR continues to decrease and changes to nMR at 100 K (see Fig. 3f and inset). Besides, as the temperature increases, the nMR initially at relatively low magnetic field quickly extends to higher field and leads to a "W" shape MR, demonstrating that the weak localization caused by electronic correlation takes over, which is the same case in $H\|ab$ configuration. Finally, the MR signal also disappears above 100 K. These results suggest that MR mechanism in the $H\perp ab$ direction is the same as that of $H\|ab$ direction; however, the orbit scattering causes much larger magnitude of pMR than that of $H\|ab$ field, which covers the FM-contributed nMR and finally leads to the acquisition of large pMR under $H\perp ab$ field configuration.

Multiple competitive and cooperative MR mechanism

$H-T$ color contour plots for the MR of $Cr_2Si_2Te_6$ are demonstrated in Fig. 4a, b, with data of the 70−100 K interval magnified in Fig. 4c, d. The similar color-scale maps between $H\|ab$ and $H\perp ab$ configurations confirm that they possess the same MR mechanisms but with different weighted contribution of positive and negative sources, as discussed above. As experimentally demonstrated above, $Cr_2Si_2Te_6$ is a vdW FMS. In addition, previous work further confirms the cooperation and interplay of electronic correlation and ferromagnetism in $Cr_2Si_2Te_6$ and its decisive role in the formation of anisotropic MR behaviors in $Cr_2Ge_2Te_6$ homologue [28,34]. Therefore, the FM interaction and electronic correlation MR mechanisms are believed to exist in $Cr_2Si_2Te_6$ and take important roles in the dualistic large MR phenomenon. Together with the Lorentz force-induced ordinary MR (i.e., orbital scattering mechanism), we therefore propose the multiple MR mechanism consisting of FM interaction, orbital scattering and electronic correlation, as schemed in Fig. 4e, which shows the relatively dominant effect in MR as a function of temperature. As demonstrated in Fig. 4e, a competition and cooperation mechanism between FM interaction, orbital scattering and electronic correlation is proposed where the FM interaction contributes nMR and dominates at temperatures below T_c, while the electronic correlation also contributes nMR but dominates in much higher temperature range and disappears above 100 K. In the intermediate temperature range, the orbit scattering-contributed pMR is more prominent, especially at high magnetic fields. The competition and cooperation between the above MR mechanisms finally give birth to the intriguing and dual-sign MR behavior observed in $Cr_2Si_2Te_6$.

The angle-dependent behaviors of MR are shown in Fig. S8. As depicted in Fig. S8a, b, with the applied field changing from 90°, 60°, 30° to 0° to the ab plane, the MR behaviors of $Cr_2Si_2Te_6$ single crystal at 25 and 40 K show a clear transition from nMR to pMR, confirming that $Cr_2Si_2Te_6$ is bestowed with an angle anisotropy in MR. Fig. S8c, d show the angular dependence of MR measured at 10 T. As shown in Fig. S8c, the absolute MR values decrease monotonically from 0° to 90° magnetic field and reach the minimum under 90° ($H\|ab$) field below 50 K. However, when the temperature is above 50 K (as shown in Fig. S8d), along with the increase of temperature, the variation trend of

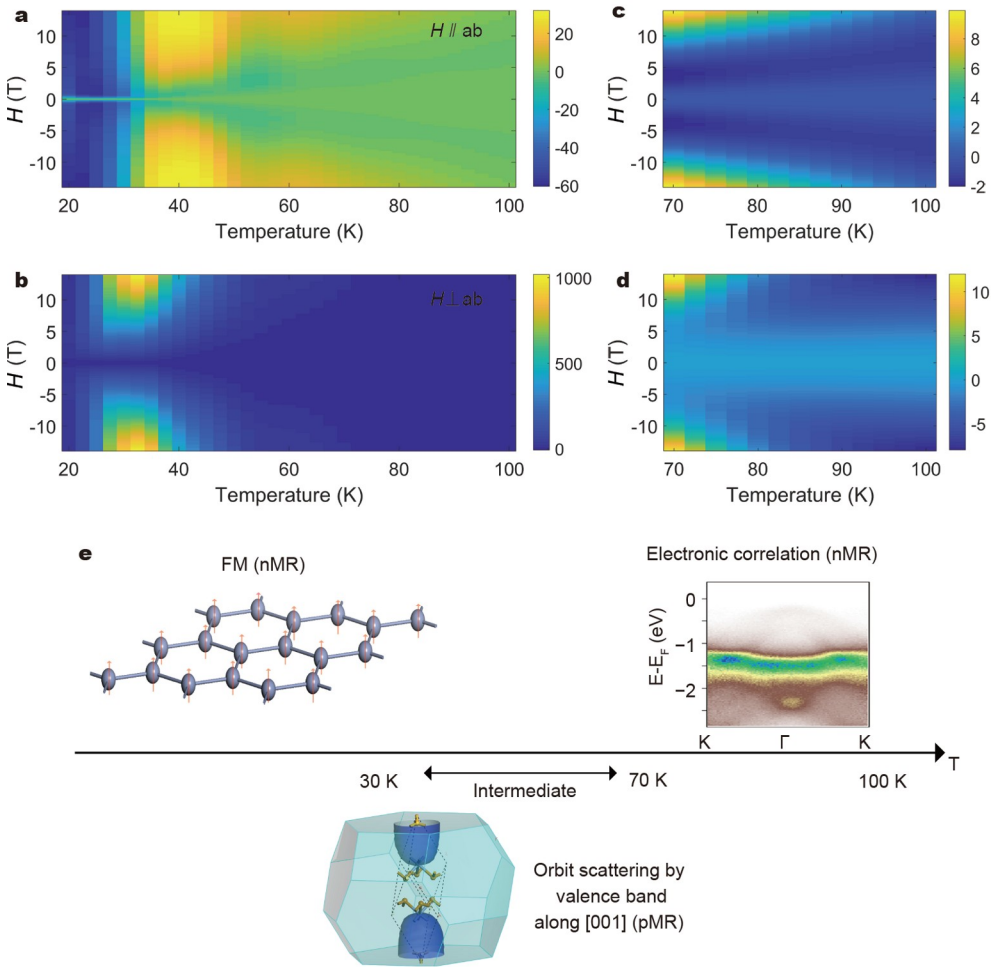

Figure 4 Mechanism for the MR effect in $Cr_2Si_2Te_6$. (a–d) *H*–*T* color contour plots for the MR of $Cr_2Si_2Te_6$ along *H*||*ab* (a, b) and *H*⊥*ab* (c, d) directions. (e) Schematic diagram of the competitive effect between FM interaction, orbit scattering, and electronic correlation, which contribute nMR, pMR, and nMR to $Cr_2Si_2Te_6$, respectively.

MR value experiences a transition from monotonic decrease to monotonic increase with field changing from 0° to 90°, and finally reaches the minimum under 0°/180° (*H*⊥*ab*) field above 80 K (see in Fig. S8d). This can be understood by comparing the MR data in Fig. 3c, f, which should be attributed to the competition and cooperation between the multiple MR mechanisms discussed above. Worthy of note is that repeatability test of the magnetotransport behavior of $Cr_2Si_2Te_6$ single crystal was made on separate samples #S2 (Fig. S9), which shows consistent results with sample #S1, proving the reliability of the data.

CONCLUSIONS

In summary, the disclosure of nMR of about −60% and pMR higher than 1000% in $Cr_2Si_2Te_6$ single crystal suggests that materials with vdW layered lattice, ferromagnetism and semiconductor natures are promising candidates for coexistence of large nMR and pMR. It is surprising that the acquisition of large and dual-sign MR is realized in this simple system. However, just like that there is a necessity in contingency, the diversity of material attributes (2D anisotropic lattice, ferromagnetism, and electronic correlation) coexisting in $Cr_2Si_2Te_6$ triggers multiple MR mechanisms, and thus fertilizes the emergence of simultaneous large pMR and nMR. Specifically, in $Cr_2Si_2Te_6$, the FM interaction, orbital scattering and electronic correlation contribute nMR, pMR, and nMR in dominated temperature and magnetic field ranges, which comprehensively leads to the acquisition of both large pMR and nMR under different field configurations. This elucidated multiple MR mechanism and coexistence of large pMR and nMR in this vdW FMS can shed light on the pursuit of coexistence of large pMR and nMR for field-sensitive device applications.

Received 16 July 2021; accepted 5 August 2021; published online 8 September 2021

1 Prinz GA. Magnetoelectronics. Science, 1998, 282: 1660–1663
2 Bai W, Hu Z, Wang S, *et al.* Intrinsic negative magnetoresistance in van der Waals $FeNbTe_2$ single crystals. Adv Mater, 2019, 31: 1900246
3 Pandey A, Mazumdar C, Ranganathan R, *et al.* Multiple crossovers between positive and negative magnetoresistance *versus* field due to fragile spin structure in metallic $GdPd_3$. Sci Rep, 2017, 7: 42789
4 Baibich MN, Broto JM, Fert A, *et al.* Giant magnetoresistance of (001) Fe/(001)Cr magnetic superlattices. Phys Rev Lett, 1988, 61: 2472–2475
5 Binasch G, Grünberg P, Saurenbach F, *et al.* Enhanced magnetoresistance in layered magnetic structures with antiferromagnetic interlayer exchange. Phys Rev B, 1989, 39: 4828–4830
6 Jin S, Tiefel TH, McCormack M, *et al.* Thousandfold change in resistivity in magnetoresistive La-Ca-Mn-O films. Science, 1994, 264: 413–415
7 Ramirez AP, Cava RJ, Krajewski J. Colossal magnetoresistance in Cr-

based chalcogenide spinels. Nature, 1997, 386: 156–159
8 Moritomo Y, Asamitsu A, Kuwahara H, *et al.* Giant magnetoresistance of manganese oxides with a layered perovskite structure. Nature, 1996, 380: 141–144
9 Lenz JE. A review of magnetic sensors. Proc IEEE, 1990, 78: 973–989
10 Daughton JM. GMR applications. J Magn Magn Mater, 1999, 192: 334–342
11 Ali MN, Xiong J, Flynn S, *et al.* Large, non-saturating magnetoresistance in WTe_2. Nature, 2014, 514: 205–208
12 Ishiwata S, Shiomi Y, Lee JS, *et al.* Extremely high electron mobility in a phonon-glass semimetal. Nat Mater, 2013, 12: 512–517
13 von Helmolt R , Wecker J, Holzapfel B, *et al.* Giant negative magnetoresistance in perovskitelike $La_{2/3}Ba_{1/3}MnO_x$ ferromagnetic films. Phys Rev Lett, 1993, 71: 2331–2333
14 Urushibara A, Moritomo Y, Arima T, *et al.* Insulator-metal transition and giant magnetoresistance in $La_{1-x}Sr_xMnO_3$. Phys Rev B, 1995, 51: 14103–14109
15 MacDonald AH, Schiffer P, Samarth N. Ferromagnetic semiconductors: moving beyond (Ga,Mn)As. Nat Mater, 2005, 4: 195–202
16 Huang C, Feng J, Wu F, *et al.* Toward intrinsic room-temperature ferromagnetism in two-dimensional semiconductors. J Am Chem Soc, 2018, 140: 11519–11525
17 Li X, Yang J. $CrXTe_3$ (X = Si, Ge) nanosheets: two dimensional intrinsic ferromagnetic semiconductors. J Mater Chem C, 2014, 2: 7071–7076
18 Lin MW, Zhuang HL, Yan J, *et al.* Ultrathin nanosheets of $CrSiTe_3$: a semiconducting two-dimensional ferromagnetic material. J Mater Chem C, 2016, 4: 315–322
19 Gong C, Li L, Li Z, *et al.* Discovery of intrinsic ferromagnetism in two-dimensional van der Waals crystals. Nature, 2017, 546: 265–269
20 Wang N, Tang H, Shi M, *et al.* Transition from ferromagnetic semiconductor to ferromagnetic metal with enhanced Curie temperature in $Cr_2Ge_2Te_6$ *via* organic ion intercalation. J Am Chem Soc, 2019, 141: 17166–17173
21 Wang Z, Gutiérrez-Lezama I, Ubrig N, *et al.* Very large tunneling magnetoresistance in layered magnetic semiconductor CrI_3. Nat Commun, 2018, 9: 2516
22 Huang B, Clark G, Navarro-Moratalla E, *et al.* Layer-dependent ferromagnetism in a van der Waals crystal down to the monolayer limit. Nature, 2017, 546: 270–273
23 Tian S, Zhang JF, Li C, *et al.* Ferromagnetic van der Waals crystal VI_3. J Am Chem Soc, 2019, 141: 5326–5333
24 Yang JH, Xiang H. Van der Waals engineering of magnetism. Nat Mater, 2019, 18: 1273–1274
25 Ouvrard G, Sandre E, Brec R. Synthesis and crystal structure of a new layered phase: The chromium hexatellurosilicate $Cr_2Si_2Te_6$. J Solid State Chem, 1988, 73: 27–32
26 Carteaux V, Moussa F, Spiesser M. 2D Ising-like ferromagnetic behaviour for the lamellar $Cr_2Si_2Te_6$ compound: A neutron scattering investigation. Europhys Lett, 1995, 29: 251–256
27 Siberchicot B, Jobic S, Carteaux V, *et al.* Band structure calculations of ferromagnetic chromium tellurides $CrSiTe_3$ and $CrGeTe_3$. J Phys Chem, 1996, 100: 5863–5867
28 Zhang J, Cai X, Xia W, *et al.* Unveiling electronic correlation and the ferromagnetic superexchange mechanism in the van der Waals crystal $CrSiTe_3$. Phys Rev Lett, 2019, 123: 047203
29 Zheng Z, Su X, Deng R, *et al.* Rhombohedral to Cubic conversion of GeTe *via* MnTe alloying leads to ultralow thermal conductivity, electronic band convergence, and high thermoelectric performance. J Am Chem Soc, 2018, 140: 2673–2686
30 Chen H, Rodrigues JNB, Rettie AJE, *et al.* High hole mobility and nonsaturating giant magnetoresistance in the new 2D metal $NaCu_4Se_4$ synthesized by a unique pathway. J Am Chem Soc, 2019, 141: 635–642
31 Liu Y, Petrovic C. Anisotropic magnetic entropy change in $Cr_2X_2Te_6$ (X = Si and Ge). Phys Rev Mater, 2019, 3: 014001
32 Casto LD, Clune AJ, Yokosuk MO, *et al.* Strong spin-lattice coupling in $CrSiTe_3$. APL Mater, 2015, 3: 041515
33 Solin SA, Thio T, Hines DR, *et al.* Enhanced room-temperature geometric magnetoresistance in inhomogeneous narrow-gap semiconductors. Science, 2000, 289: 1530–1532
34 Liu W, Wang Y, Han Y, *et al.* Anisotropic magnetoresistance behaviors in the layered ferromagnetic $Cr_2Ge_2Te_6$. J Phys D-Appl Phys, 2020, 53: 025101

Acknowledgements This work was financially supported by the National Natural Science Foundation of China (U1832142 and 21805269), the National Key R&D Program of China (2018YFB0703602 and 2017YFA0303500), the Youth Innovation Promotion Association, CAS (Y202092), the Fundamental Research Funds for the Central Universities (WK2340000094), The University Synergy Innovation Program of Anhui Province (GXXT-2020-003), Anhui Provincial Natural Science Foundation (1808085QA08), the Key Research Program of Frontier Sciences (QYZDY-SSW-SLH011), China Postdoctoral Science Foundation (2017M620261, 2019TQ0293 and 2020M671868), and the National Synchrotron Radiation Laboratory Joint funds of University of Science and Technology of China (KY2060000156 and KY2340000114).

Author contributions Xiao C, Li Z, Bai W and Xie Y conceived the idea and co-wrote the paper; Li Z, Li Y and Zhang W carried out the sample synthesis and basic characterization; Li Z, Bai W and Zhao J carried out the physical magnetic and magnetotransport measurements; Li Y, Wang S and Sun Z recorded the angle-resolved photoemission spectroscopy data and made an interpretation; Xie Y, Xiao C, Li Z, Bai W and Sun Z discussed the magnetotransport mechanism. All the authors contributed to the overall scientific interpretation and edited the manuscript.

Conflict of interest The authors declare no conflict of interest.

Supplementary information Supporting data are available in the online version of the paper.

Zhou Li obtained his BSc degree from Wuhan University of Technology in 2012 and PhD degree from the University of Science and Technology of China (USTC) in 2017. Then, he took a postdocral research at USTC from 2017 to 2020. He is now an associate professor at Anhui University. His current research interests include high-performance thermoelectric materials and the thermal/electrical/magnetic transport properties of inorganic functional solids.

Wei Bai received his PhD degree from USTC in 2019. He is now an associate researcher of Hefei National Laboratory for Physical Sciences at the Microscale, USTC. His recent interests include the physical properties of ternary chalcogenides and their applications in energy conversion.

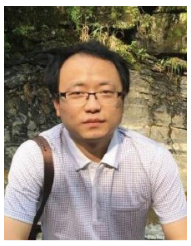

Chong Xiao obtained his PhD degree from USTC in 2013. He is now a professor of Hefei National Laboratory for Physical Sciences at Microscale, USTC. He has been working on advanced energy conversion materials more than ten years, from materials synthesis and characterization to understanding the underlying physics and chemistry mechanism. His recent research interests focus on the design and synthesis of low-dimensional inorganic solids with efforts to modulate their electron and phonon structures for energy storage and conversion applications.

$Cr_2Si_2Te_6$铁磁半导体中大的正、负磁阻共存现象

李周[1†], 白巍[1†], 李昱良[3], 李渊龙[1], 王盛[3], 张炜辉[1], 赵继印[1], 孙喆[3], 肖珅[1,2*], 谢毅[1,2]

摘要 磁阻(MR)作为一种电子输运与磁场耦合的宏观现象，一直是凝聚态物理和材料科学的研究前沿. 其中, 大的磁阻现象及材料对磁传感器和信息存储应用尤为重要，而这种材料的稀缺也引起了人们的广泛关注. 此外，由于物理起源不同，在一种化合物中同时存在大的正、负磁阻少见报道. 本工作中，我们在$Cr_2Si_2Te_6$铁磁半导体单晶中实现了不同磁场方向下大的正磁阻(pMR)和负磁阻(nMR)共存. 具体而言，在面内场方向获得了约−60%的大的nMR，在面外场方向获得了高于1000%的大的pMR. 我们将这种磁场方向依赖的磁阻行为归因于$Cr_2Si_2Te_6$中的铁磁相互作用、轨道散射和电子关联作用的竞争和合作效应，它们在相应温度和磁场范围内分别使$Cr_2Si_2Te_6$表现出nMR，pMR和nMR. 阐明这种铁磁半导体中的磁阻机制将为寻求大的pMR和nMR共存的磁场敏感器件提供指导.

